

# Three-dimensional optical coherence tomography of the embryonic murine cardiovascular system

**Wei Luo**

**Daniel L. Marks**

University of Illinois at Urbana-Champaign  
Beckman Institute for Advanced Science  
and Technology  
Urbana, Illinois 61801

**Tyler S. Ralston**

University of Illinois at Urbana-Champaign  
Beckman Institute for Advanced Science  
and Technology  
Department of Electrical and Computer Engineering  
Urbana, Illinois 61801

**Stephen A. Boppart**

University of Illinois at Urbana-Champaign  
Beckman Institute for Advanced Science  
and Technology  
Departments of Electrical and Computer Engineering,  
Bioengineering, and Medicine  
Urbana, Illinois 61801  
E-mail: boppart@uiuc.edu

**Abstract.** Optical coherence tomography (OCT) is an emerging high-resolution real-time biomedical imaging technology that has potential as a novel investigational tool in developmental biology and functional genomics. In this study, murine embryos and embryonic hearts are visualized with an OCT system capable of 2- $\mu\text{m}$  axial and 15- $\mu\text{m}$  lateral resolution and with real-time acquisition rates. We present, to our knowledge, the first sets of high-resolution 2- and 3-D OCT images that reveal the internal structures of the mammalian (murine) embryo (E10.5) and embryonic (E14.5 and E17.5) cardiovascular system. Strong correlations are observed between OCT images and corresponding hematoxylin- and eosin-stained histological sections. Real-time *in vivo* embryonic (E10.5) heart activity is captured by spectral-domain optical coherence tomography, processed, and displayed at a continuous rate of five frames per second. With the ability to obtain not only high-resolution anatomical data but also functional information during cardiovascular development, the OCT technology has the potential to visualize and quantify changes in murine development and in congenital and induced heart disease, as well as enable a wide range of basic *in vitro* and *in vivo* research studies in functional genomics. © 2006 Society of Photo-Optical Instrumentation Engineers. [DOI: 10.1117/1.2193465]

**Keywords:** imaging; optical coherence tomography; cardiovascular malfunction; embryology; functional genomics.

Paper 05129SSR received Jun. 1, 2005; revised manuscript received Sep. 18, 2005; accepted for publication Sep. 26, 2005; published online Apr. 18, 2006.

## 1 Introduction

Embryonic development is a complex process with rapid dynamic changes. Defects in developmental mechanisms during embryogenesis have long been thought to result in congenital cardiac abnormalities. Congenital heart defects (CHDs) are present in about 1% of live births in the United States and are the most common congenital malformations in newborns.<sup>1</sup> A total of 4109 deaths due to CHDs were recorded in 2001.<sup>1</sup> Our current understanding of abnormal developmental processes that lead to CHDs is limited. The ability to analyze the organization of biological tissue in 3-D, and the resultant function of the developing morphology, has the potential to provide invaluable information that could lead to a better fundamental understanding and possibly a reduction of CHDs.

A number of technologies have been developed for obtaining 3-D information from biological tissues at various size scales. Traditional serial sectioning histology can be laborious and time consuming, frequently requiring the viewing and photographing of hundreds of physical sections to gain an appreciation of complex 3-D structures.<sup>2</sup> Other techniques can intrinsically collect 3-D volumes and include magnetic resonance imaging (MRI), tissue Doppler gating, ultrasound backscatter microscopy, surface imaging microscopy, confocal mi-

croscopy, optical projection tomography (OPT), confocal microscopy, and optical coherence tomography (OCT). High-field MRI is excellent for imaging larger but fixed tissue specimens and 25- to 31- $\mu\text{m}$  resolution is achievable with long scan times and large magnetic fields.<sup>3</sup> Fast gradient echo sequence MRI has been used to identify cardiac malformations with resolutions on the order of 60 to 75  $\mu\text{m}$ , but even with speed improvements, this method still requires overnight acquisition.<sup>4</sup> Tissue Doppler gating can achieve 3-D fetal heart imaging with high temporal and spatial resolution, but the results are highly influenced by operator expertise.<sup>5</sup> Ultrasound backscatter microscopy was used to study live murine embryos *in utero* between 9.5 and 11.5 days of embryogenesis but with a spatial resolution close to 50  $\mu\text{m}$ .<sup>6</sup> Surface imaging microscopy can perform 3-D embryo imaging with high resolution, but samples need to be fixed, labeled, and embedded. The entire imaging process, from loading the block to finishing the image collection, requires approximately 3 to 6 h.<sup>7</sup> OPT is a new technique related to computed tomography that images fixed, relatively large samples that have been made optically transparent. OPT, however, is not well suited for specimens that contain optically dense and highly scattering tissues such as cartilage or bone, and the technique has not shown cellular-resolution imaging.<sup>8</sup> Advanced microscopy techniques, such as confocal and multi-

Address all correspondence to Stephen Boppart, University of Illinois at Urbana-Champaign, Beckman Institute, 405 N. Mathews Ave., Urbana, IL 61801. Tel: 217-244-7479; Fax: 217-244-1995; E-mail: boppart@uiuc.edu

photon microscopy, can image to limited depths of several hundreds of microns and typically rely on the detection of fluorescent signals from exogenous probes.<sup>9</sup> Because optical methods do not necessarily require the tissue to be fixed, the alteration to the tissue structure is minimized before imaging.

Optical coherence tomography (OCT) is an emerging high-resolution imaging technology that uses near-infrared wavelengths to perform optical ranging in a manner analogous to ultrasound imaging but with resolutions one to two orders of magnitude higher due to the shorter wavelengths of light.<sup>10,11</sup> While depth of imaging is limited to a few millimeters in highly scattering tissues, OCT imaging resolutions less than 1  $\mu\text{m}$  have been demonstrated.<sup>12</sup> OCT generates cross sectional images representing the spatially localized intensity of optical backscatter, typically without the addition of exogenous dyes or probes. Remarkably, the stained morphological features in histology correspond extremely well with the endogenous backscattering features detected in OCT, even though the light propagation through the tissue for each technique is in orthogonal directions. The use of OCT could therefore be a powerful alternative to standard histological processing for the investigation of embryogenesis in the field of developmental biology.<sup>13,14</sup> The OCT technology can image the internal structures of the embryonic cardiovascular system with high resolution in 2-D and 3-D, and has previously been applied for the assessment of the developing cardiovascular systems in *Xenopus laevis* (the African frog) and the chick.<sup>13,14</sup>

The mouse, due to its small size, ease of care and handling, prolific reproductive ability, short gestational period, and well-known genotype, is one of the most established research animal models.<sup>15,16</sup> With its well-characterized genotype, and the successful use of targeted mutagenesis and knock-out studies in functional genomics, the murine model plays a vital role in exploring the genetic basis, etiology, and therapy of human disease. Functional measurements of early mammalian cardiac development are rare, because the mammalian embryo is not easily accessible for experimental manipulation. Therefore, our primary motivation for this study was to image and analyze developing embryonic mammalian cardiovascular morphology and function in a unique way by using OCT.

In this work, we demonstrate, to the best of our knowledge, the first OCT imaging of *in vitro* and *in vivo* embryonic mice, and in particular, the murine cardiovascular system. We present a series of 3-D OCT datasets of mouse embryos and embryonic hearts at different gestational stages, along with corresponding hematoxylin and eosin (H and E)-stained histological sections. These data include static OCT images of whole murine embryos at embryonic day 10.5 (E10.5), and dissected embryonic hearts at days E14.5 and E17.5. The data also include real-time functional images of beating embryonic hearts from an E10.5 embryo. We demonstrate, at three different gestational stages, that the practical resolution of OCT is sufficient to image 3-D developing morphology in whole embryos with histological-level resolution, without having to histologically process, section, and stain tissue.

## 2 Materials and Methods

### 2.1 Animal Preparation

All animal procedures were performed according to the approved protocols of the Institutional Animal Care and Use Committee at the University of Illinois at Urbana-Champaign. Swiss Webster mice were purchased (Harlan, Indianapolis, Indiana) at 6 to 8 weeks of age. The paired breeding system was used and the presence of a vaginal plug indicated copulation.<sup>17</sup> Fertilization was assumed and gestational dating of day 0.5 was assigned. Females were subsequently placed in separate cages for the remainder of gestation.

### 2.2 Embryo Preparation for Static Imaging

Pregnant females were euthanized by CO<sub>2</sub> inhalation at desired gestational age and the maternal abdomen was incised. The uterus was gently retracted out of the abdominal cavity and embryos were dissected from the uterus and placed in a petri dish. For E14.5 and E17.5 embryos, the chest cavity was opened and the pericardium was removed to expose the heart. During OCT imaging, whole embryos (E10.5) or embryos with exposed hearts (E14.5 and E17.5) were immersed in saline. At each gestational age, three embryo specimens were imaged and multiple stacks, comprising 3-D volumes of OCT image data, were recorded.

### 2.3 Embryo Preparation for Dynamic Imaging

Immediately following euthanasia of the pregnant mouse, the entire uterus was gently retracted from the abdominal cavity and one half of the uterus was opened to expose embryos still in intact amnion sacs. Partially exposed embryos were immersed in warmed saline for real-time spectral-domain OCT imaging. Embryo-placental continuity was maintained, and embryos remained *in situ*, encased in the amnion sac and filled with amniotic fluid. *In situ* embryos remained warm from the body temperature of the euthanized pregnant mouse. No additional effort was made to maintain normothermia of the embryos. This *in situ* approach was used to yield more physiologically relevant functional data.

### 2.4 Optical Coherence Tomography

3-D OCT imaging was performed using a neodymium:vandate diode-pumped titanium:sapphire laser as a low-coherence light source. The pulsed laser output had a center wavelength at 800 nm with a 100-nm spectral bandwidth at a pulse repetition rate of 90 MHz and an average output power of 350 mW, which enabled an axial imaging resolution of approximately 2  $\mu\text{m}$  in tissue. This light was coupled into a fiber optic coupler that served as a beamsplitter in this fiber-optic-based OCT system (Fig. 1). The sample arm light from the fiber was collimated, reflected off a pair of orthogonal galvanometer-mounted mirrors that directed the *x-y* position of the beam on the tissue, and was focused by a 20-mm focal length achromatic lens to a spot size diameter (transverse resolution) of 15  $\mu\text{m}$ , with a confocal parameter of 400  $\mu\text{m}$ . Incident optical power on the tissue was measured to be 10 mW. The time-domain OCT instrument included a reference arm with a galvanometer-mounted retroreflecting mirror translated over an optical pathlength of 1.5 mm at a frequency of 40 Hz. Reflections from each interferometer arm

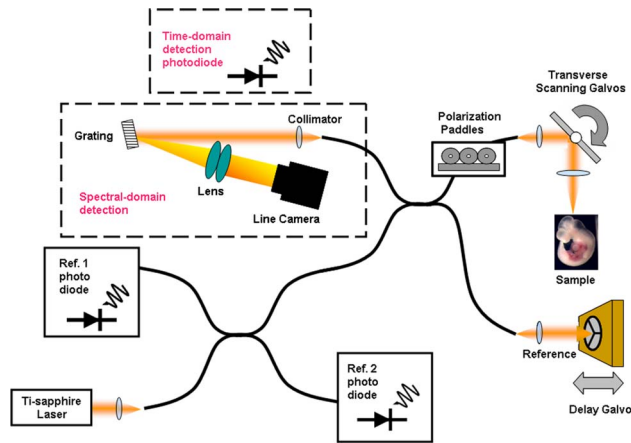


**Fig. 1** Schematic of the time-domain optical coherence tomography (TD-OCT) and the spectral-domain optical coherence tomography (SD-OCT) systems. The two systems use the same source and sample arm. TD-OCT uses a photodetector and a moving reference-arm mirror, while SD-OCT uses a spectral detector and a stationary reference-arm mirror.

were recombined in the fiber optic coupler and the interference signal was sensed by a photodiode. A second reference photodiode was used to monitor laser power fluctuations and was subtracted from the signal photodiode to cancel these fluctuations. The electrical output of the photodiode was bandpass filtered, amplified, and digitized with 12-bit accuracy. OCT volume scans were performed by acquiring sequential cross sectional ( $x$ - $z$ ) scans at  $10\text{-}\mu\text{m}$  intervals along the  $y$  axis. Custom software assembled digital data for display as 2-D or 3-D images. 2-D images ( $512 \times 512$  pixels) were acquired in 17 s with the slower time-domain OCT method, and 3-D datasets consisting of 256 2-D images were acquired in about 70 min. Faster acquisition rates are possible using advanced time-domain scanning methods (64 ms per image, 16.4 s per 3-D dataset)<sup>18</sup> at the expense of lower signal-to-noise ratios, or by using swept-source<sup>19</sup> or spectral-domain OCT techniques. Custom previously published image processing algorithms were applied to enhance the visualization of morphological features at high resolutions.<sup>20</sup>

### 2.5 Spectral-Domain Optical Coherence Tomography

Spectral-domain optical coherence tomography (SD-OCT) is an emerging technique that rapidly generates an OCT image from the spectrum of the light backscattered off of the sample.<sup>21,22</sup> The advantage of this technique is an increased signal-to-noise ratio (SNR) at a higher acquisition rate.<sup>21</sup> Figure 1 shows features of our SD-OCT system. The source and sample arm are equivalent to those used in the time-domain (TD) OCT system described before. The main differences found in the SD-OCT system compared to the TD-OCT system are that the reference arm is held stationary rather than scanned for depth imaging, and that a spectrometer (linear detector array) is used to capture the optical spectrum of the returning light, rather than a single element photodiode. In the SD-OCT system, the light returning from the sample and reference arms was directed into the spectrometer. Light was dispersed off of a diffraction grating (830.3 grooves/mm) and focused using a pair of achromatic lenses which have a

combined focal length of 150 mm. The focused light was incident on a line-scan camera (L104k-2k, Basler, Incorporated, Ahrensburg, Germany) containing a 2048-element array of detection elements. This camera has a maximum readout rate of 29 kHz, thus one axial (depth) scan can be captured in  $34\ \mu\text{s}$ . Digital processing of the detected signal included a spline interpolation to make the signal more uniform, and a discrete Fourier transform on each set of 2048 10-bit values to transform the signal from the frequency (spectral) domain into the spatial (depth) domain. Each scan contained data for one axial (depth) scan. Adjacent axial scans were assembled into 2-D cross sectional images for visualization on a personal computer.

It should be noted that in the present instrument, the axial resolution is superior to the transverse resolution. High axial resolution can be used to ameliorate speckle by averaging the amplitudes of several speckles over a particular feature size. Alternatively, one could use a higher transverse resolution at the expense of a shorter depth of field, and then employ focus tracking or acquire several depth scans to stitch together an image. Our resolution dimensions were chosen on the basis of available instrumentation and murine cardiac feature sizes.

### 2.6 Tissue and Image Analysis

During OCT imaging, approximately 256 images per specimen were acquired. Following OCT imaging, specimens were fixed in 10% neutral buffered formalin, followed by standard paraffin preparation. Since histological sectioning can only represent one plane per sample, two additional littermates of the imaged E10.5 embryo were histologically processed and sectioned at planes that corresponded to the computationally extracted 2-D OCT image planes. Sections ( $6\ \mu\text{m}$  thick) were stained with H and E according to standard protocol for light microscopy observation (BH-2, Olympus America, Incorporated, Melville, NY) and digital image capture (Spot RT Slider, Diagnostic Instruments, Sterling Heights, MI). Comparisons were made between matched OCT and light microscopy images, correlating microstructural features.

OCT images contained within 3-D datasets were first processed using custom dispersion compensation algorithms,<sup>20</sup> then processed using the linear burn algorithm (Photoshop 7.1, Adobe Systems, Incorporated, San Jose, CA) to compensate for depth-dependent signal attenuation, and then viewed and analyzed using commercial software (Analyze<sup>®</sup>, Biomedical Imaging Resource, Mayo Clinic, Rochester, MN and Amira<sup>®</sup>, ZIB, Mercury Computer Systems, Berlin, Germany) on a personal computer. 3-D projections and volume-rendered datasets were generated and rotated along  $x$ - $y$ - $z$  coordinates for visualization of microstructural features. Using volume data, three different planes of images were formed, consisting of a transverse plane (cross sectional depth plane), a sagittal plane, and an oblique plane, relative to the long axis of the embryo. Acquired data are presented in three formats: 1. extracted 2-D images at selected planes, 2. flipbook movies (QuickTime Version 6.5.2), and 3. volumetric renderings of the whole mouse embryo (E10.5) and embryonic hearts (E14.5 and E17.5). All movie files and captions can be viewed at: <http://biophotonics.uiuc.edu/movies/mouseembryo/>.

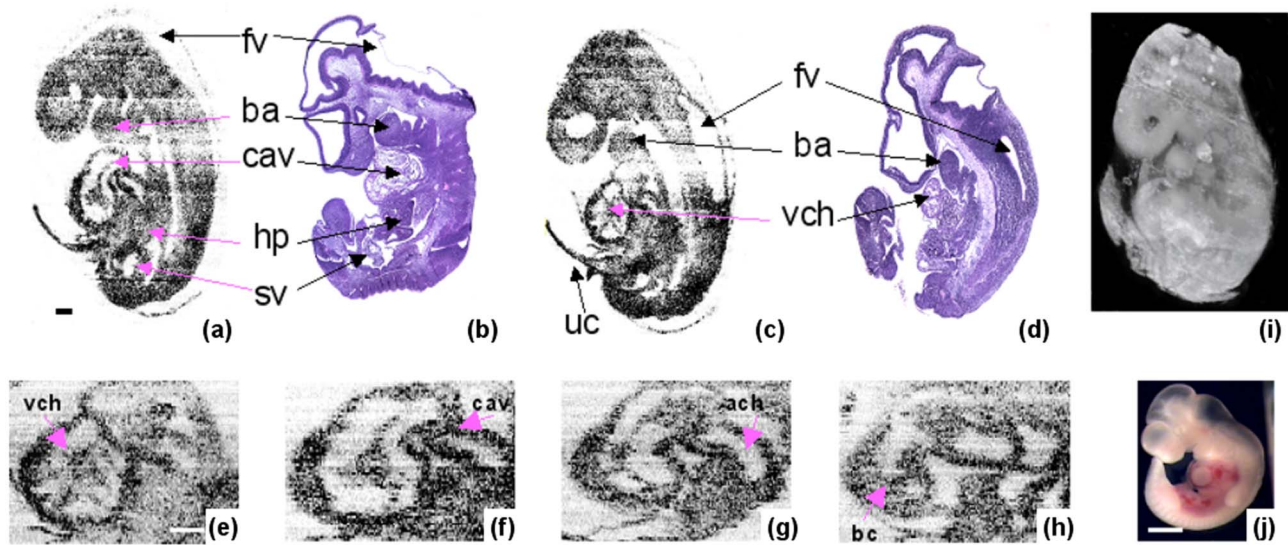


**Fig. 2** Sagittal OCT images of the E10.5 mouse embryo. (a) and (c) Computational sections along sagittal planes extracted from the 3-D OCT dataset. (b) and (d) Corresponding H and E-stained histological sections. (e) through (h) Zoomed OCT images of the embryonic heart, showing details of internal structures at varying cross sectional planes. (i) 3-D volume rendering of the OCT dataset. (j) Digital photograph of the E10.5 mouse embryo that was imaged with OCT. The entire set of 256 2-D sagittal OCT images can be viewed in Movie I. Abbreviations: ba, branchial arch; hp, hepatic primordia; fv, fourth ventricle; sv, subcardinal vein; vch, ventricular chamber; cav, cushion tissue lining the atrio-ventricular canal; ach, atrial chamber; bc, bulbus cordis; and uc, umbilical cord. Scale bars=200  $\mu\text{m}$  (a) through (d) and (i); 100  $\mu\text{m}$  (e) through (h); and 1 mm (j).

### 3 Results

#### 3.1 Optical Coherence Tomography Imaging of Static E10.5 Murine Embryo

A fresh whole embryo (E10.5) was imaged by OCT. Images from three different cross sectional planes from a 3-D OCT dataset are shown in Figs. 2–4. OCT is capable of resolving the internal structures of the embryo with high resolution (2- $\mu\text{m}$  axial, 15- $\mu\text{m}$  transverse) and as deep as 1 mm in the highly scattering tissue of the embryo. A 3-D OCT dataset containing 256 2-D OCT images was computationally sectioned along the sagittal plane of the embryo, and shown with corresponding histological sections in Fig. 2. The optical sectioning capability and the high resolution are apparent. Despite the optically dense and highly scattering structures of the

murine embryo (estimated at 10 to 20-dB/mm attenuation), features are well preserved at depths up to 1 mm in the specimen and strongly correlated with the H and E-stained histological sections at comparable planes. The representative sagittal images in Fig. 2 present many detailed internal structures including the branchial arch, hepatic primordia, fourth ventricle, and subcardinal vein. Figures 2(e)–2(h) are zoomed-in regions of acquired OCT images and show the anatomic structures of the embryonic heart including the bulbus cordis, the cushion tissue lining the atrio-ventricular canal, and an atrial and ventricular chamber of the heart. The high resolution and structural representation through the whole embryo clearly illustrate the developing cardiovascular and nervous system, among others. In Figs. 2(i) and 2(j), a

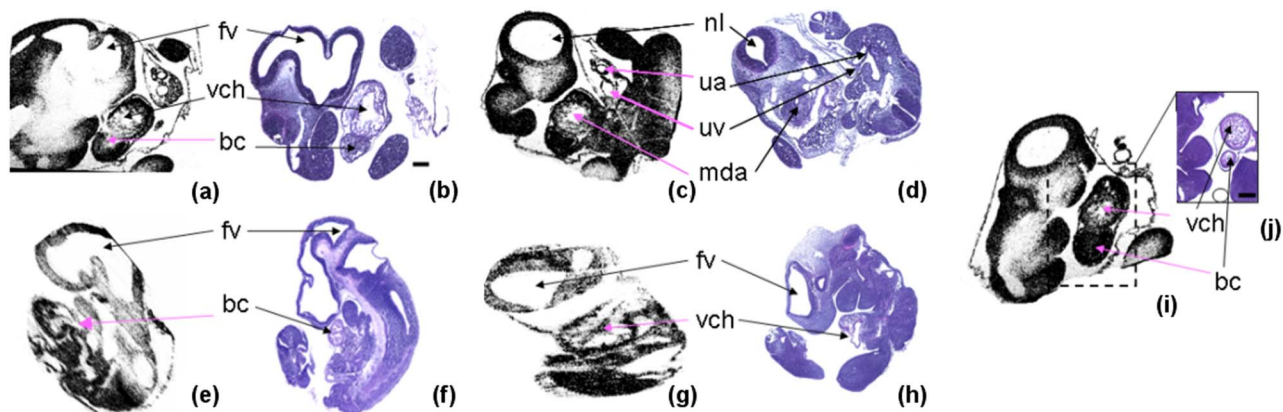


**Fig. 3** Oblique OCT images of the E10.5 mouse embryo. (a), (c), (e), (g), and (i) Computational sections along oblique planes extracted from the 3-D dataset. (b), (d), (f), (h), (j) Corresponding H and E-stained histological sections. Abbreviations: nl, neural lumen; bc, bulbus cordis; vch, ventricular chamber; fv, fourth ventricle; mda, middle line dorsal aorta; uv, umbilical vein; and ua, umbilical artery. Scale bar=200  $\mu\text{m}$ .

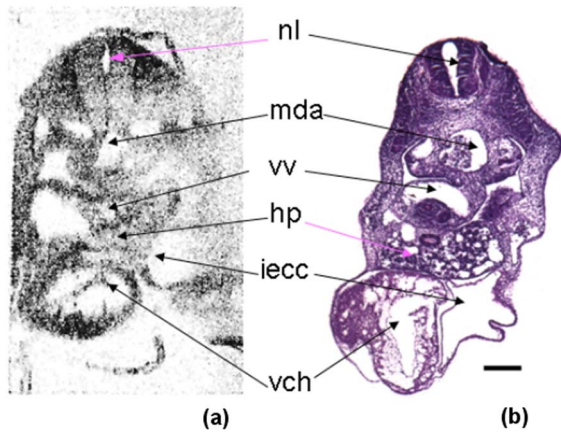


**Fig. 4** Transverse OCT images of the E10.5 mouse embryo. One section (out of 256 2-D OCT images) of a whole E10.5 murine embryo is shown, and represents the imaging plane at which the original 2-D OCT images were acquired serially to assemble the 3-D OCT dataset. (a) OCT image and (b) corresponding H and E-stained histological section. The entire 256 OCT image set is presented as a flipbook movie (see Movie II). Abbreviations: nl, neural lumen; mda, midline dorsal aorta; vv, vitelline vein; hp, hepatic primordia; iecc, intra-embryonic coelomic cavity; and vch, ventricular chamber. Scale bar = 200  $\mu\text{m}$ .

3-D volume-rendered image from the 3-D OCT dataset is compared with a digital image of the murine embryo (E10.5) used to generate this dataset. A sequence of 256 computationally sectioned OCT images along the sagittal plane is presented as the flipbook Movie I.

To illustrate and identify other anatomical structures, the 3-D OCT dataset was also computationally sectioned at an oblique plane and shown in Fig. 3, along with corresponding histological sections. From these oblique images, structures

identified include the neural lumen, bulbus cordis, a ventricular chamber of the heart, fourth ventricle, and the mid-line dorsal aorta. Finally, one representative transverse OCT section from the set of 256 is shown in Fig. 4, along with the corresponding H and E-stained histological section. The section was acquired transverse to the long axis of the embryo and represents the original plane at which 2-D OCT images were acquired in series to assemble the 3-D OCT dataset. A sequence of all 256 images can be viewed as a flipbook (Movie II). Depth-dependent attenuation of the OCT signal intensity is evident in these images. Relative to the orientation of these OCT images, the imaging beam was incident left to right. These depth-dependent attenuation effects appear as lighter, faded regions in the right half of this OCT image. This effect is dependent on the direction of the incident OCT imaging beam, relative to the regional optical properties of the specimen, and can be mediated by imaging at varying angles around structures of interest.

### 3.2 Optical Coherence Tomography Imaging of Static E14.5 and E17.5 Murine Embryos

Exposed hearts from E14.5 and E17.5 embryos were prepared and imaged. Figure 5 illustrates oblique images extracted from the 3-D OCT volume and the corresponding histology. In these images, cardiac structures including an atrial chamber, a ventricular chamber, a ventricular outflow tract, and the aorta and pulmonary trunk can be clearly visualized. The heart from a relatively late developmental stage (E17.5) was also imaged. Figures 5(f) and 5(h) are OCT images that reveal defined cardiovascular structures such as the atria, ventricles, and the aorta, which are confirmed in the strongly correlating histology in Figs. 5(g) and 5(i). Figures 5(e) and 5(j) are 3-D volume-rendered images of the embryonic murine hearts at days E14.5 and E17.5, respectively, which clearly show the

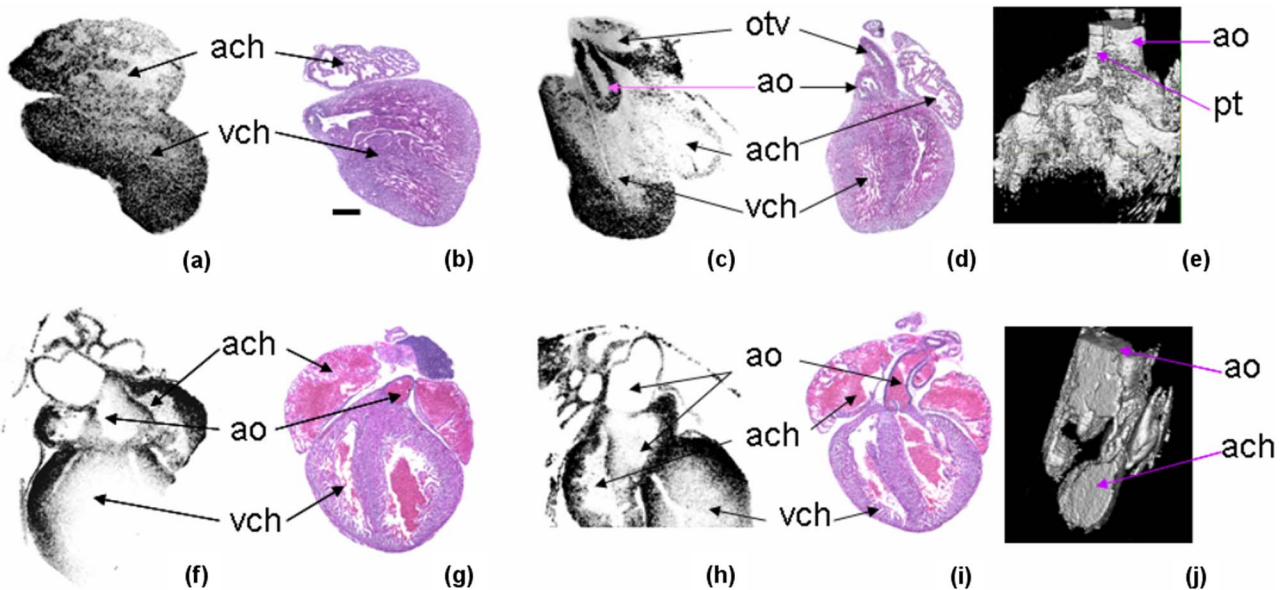


**Fig. 5** OCT of the embryonic mouse heart (E14.5 and E17.5). (a) and (c) OCT images, (b) and (d) corresponding H and E-stained histology, and (e) 3-D OCT volume rendering of the E14.5 murine heart. (f) and (h) OCT images, (g) and (i) corresponding histology, and (j) 3-D OCT volume rendering of the E17.5 murine heart. Abbreviations: ach, atrial chamber; vch, ventricular chamber; otv, outflow tract of ventricle; ao, aorta; and pt, pulmonary trunk. Scale bar = 200  $\mu\text{m}$ .

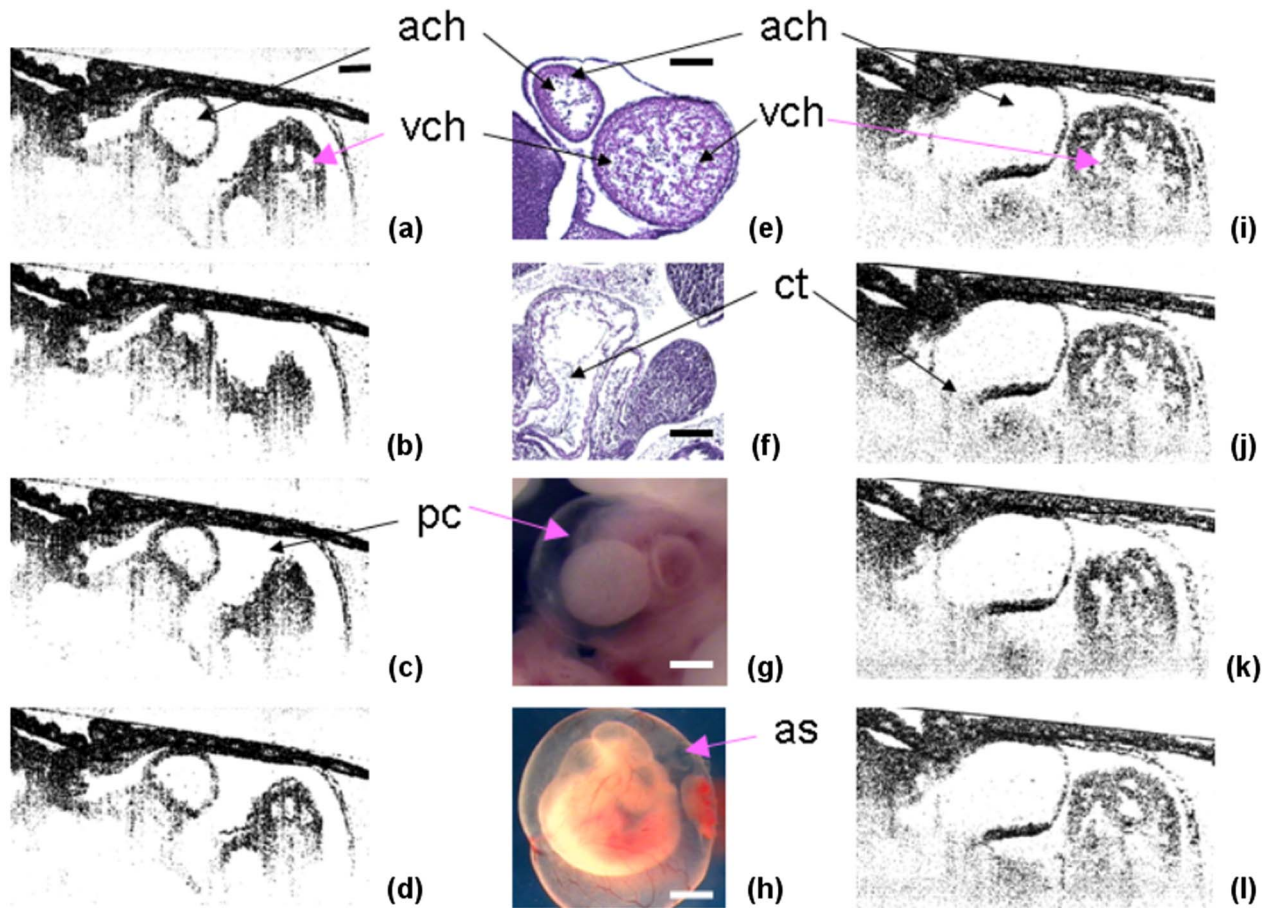


**Fig. 6** *In vivo* OCT imaging of the beating E10.5 murine heart. (a) through (d) and (i) through (l) Sequences of four serial frames extracted from movies captured using SD-OCT. Each sequence was acquired from a different angle (acquired 5 frames/sec, see Movies III and IV). The dynamic motion of the E10.5 heart is evident: (a) early systole, (b) end-systole, (c) early diastole, and (d) end diastole. (e) and (f) Corresponding H and E-stained histology for (a) through (d) and (i) through (l) sequences, respectively. (g) Digital photograph of the highly scattering embryonic heart. (h) Digital photograph of the murine embryo encased in an intact amnion sac filled with amniotic fluid, the condition under which OCT images were acquired. Abbreviations: ach, atrial chamber; vch, ventricular chamber; ct, cushion tissue; pc, pericardial cavity; and as, amnion sac. Scale bars=200  $\mu\text{m}$  (a) through (g) and (i) through (l) and 1 mm (h).

major vasculature surrounding the heart, including the pulmonary trunk and the aorta.

### 3.3 Optical Coherence Tomography Imaging of Dynamic E10.5 Murine Embryo

The SD-OCT system enabled continuous data acquisition, processing, and display at five frames per second, which was suitable for *in vivo* optical imaging. *In vivo* murine embryo (E10.5) heart rates have been reported to be approximately 120 to 210 beats per minute,<sup>23,24</sup> which corresponds to 4 to 7 frames/sec imaging required to acquire two frames per beat, and 5 frames/sec is sufficient to image up to 150 beats/min with two frames per beat. In this study, semi-exposure of the E10.5 embryo maintained embryo-placental continuity, and the embryo remained *in situ*, encased in its amnion sac and amniotic fluid [Fig. 6(h)]. This semi-invasive approach was taken to yield more physiologically relevant data. However, due to maternal-embryo euthanasia, specimen preparation, and the semi-invasiveness of this protocol, the heart rate slowed to 20 to 30 beats/min prior to imaging.

Figures 6(a)–6(d) are four serial frames extracted from a SD-OCT movie (Movie III). The dynamic motion of the E10.5 heart is shown at varying stages of the cardiac cycle, including: early systole [Fig. 6(a)] end systole [Fig. 6(b)], early diastole [Fig. 6(c)] and end diastole [Fig. 6(d)]. Figures 6(i)–6(l) are four serial frames extracted from a SD-OCT movie (Movie IV) captured at a different position and angle. The dynamic motion of the cardiac cushion of the E10.5 heart was observed. The corresponding histology for the image sequences is also shown. Figure 6(g) is a digital photograph of the surface of the highly scattering embryonic heart, shown in the orientation in which the OCT imaging beam was incident. Figure 6(h) is a digital image of the whole murine embryo encased in its amnion sac and surrounded by amniotic fluid, through which OCT imaging was performed.

## 4 Discussion

In summary, we have demonstrated, to the best of our knowledge, the first OCT imaging of *in vitro* and *in vivo* embryonic mice, and in particular, the murine cardiovascular system.

OCT was capable of obtaining high-resolution images and 3-D datasets of both static (E14.5 and E17.5) and dynamic (E10.5) murine embryonic hearts, as well as static images of a whole embryo (E10.5). The OCT images and the computational sections from 3-D datasets correlate strongly with corresponding histological sections and show many internal morphological details. The 2-D OCT images and 3-D OCT datasets acquired and analyzed from fresh specimens represent a novel investigative technique and potentially a time- and cost-saving method for the morphological analysis of the complex developing murine cardiovascular system, without the need to fix and histologically process tissue, photograph H and E-stained slides, register sections, and digitally reconstruct 3-D volumes. Furthermore, real-time dynamic motion of the atria, ventricles, and cardiac cushion in the E10.5 embryonic heart was captured by SD-OCT.

As an emerging and potentially powerful imaging modality, OCT enables depth-resolved, noninvasive and nondestructive investigations of tissue morphology and function, and has been applied in a wide range of biological and medical investigations, notably in the field of developmental biology.<sup>13,14</sup> OCT systems can be compact, fast, optically stable, easy to use, and readily configured with standard light microscopes. OCT overcomes many of the obstacles of conventional 2-D histology and 3-D visualization in developmental studies. OCT can efficiently achieve optical sectioning and imaging without the use of additional exogenous stains or probes, a key feature for the study of live embryonic development. Recent research, however, has been focused on the development of novel optical contrast agents and methods specifically for OCT.<sup>25,26</sup> These could be used to potentially label specific cell types within developing specimens, or for tracking cell fates or migration pathways. In addition to morphological imaging, OCT can visualize and quantify functional information, which is obviously lost in histology.

In this study, OCT performed nondestructive optical sectioning, capturing 3-D datasets of murine embryos and embryonic cardiovascular systems with high resolution. Many internal morphological details throughout the specimens were visualized, with strong histological correlation. Frequently, critical 3-D anatomical relationships may be lost with histological dissection and sectioning, particularly in complex vascular networks. The acquisition of a 3-D OCT dataset from the E10.5 murine embryo enabled the virtual computational sectioning of the 3-D dataset along any orientation or plane (Figs. 2 and 3, and Movie I), allowing full visualization of the morphology in embryogenesis with resolutions approaching that of standard histology, and potentially reducing the need for processing large numbers of specimens.

Imaging of the embryonic murine heart *in situ* and under physiological conditions is not trivial, since anatomical structures are small, relatively inaccessible, and dynamic at rapid heart rates. Therefore, high spatial and temporal resolutions are fundamental requirements for embryonic murine cardiac imaging. With the high-speed acquisition capabilities afforded by SD-OCT, and the potential to image at higher rates, it will likely be possible to image the development of the murine cardiovascular system at selected time points both morphologically and functionally in an *in situ* embryo. The time-domain OCT method used to acquire 3-D OCT data is a commonly used and well-established method suitable for image

acquisition from static specimens. The SD-OCT method is a relatively new modification for real-time acquisition, but can suffer from a lower SNR at greater depths due to the modulation transfer function of the spectral detection. The speed and SNR improvements available with SD-OCT help to integrate the visualization of morphological interactions in 3-D space with those changes over time.

OCT provides many advantages for imaging the embryonic murine cardiovascular system; however, as with any imaging technique, there are limitations. Future technical challenges to address these limitations include potentially improving the depth of imaging by using longer wavelength low-coherence optical sources, accessing more physiologically relevant functional data, and performing Doppler OCT. Imaging depth in OCT is limited by light scattering and absorption, which are dependent on the wavelength of the light and the optical properties of the tissue. The depth-dependent attenuation of the OCT signal intensity appears as lighter, faded regions. This effect is dependent on the direction of the incident OCT imaging beam and can be mediated by imaging near structures of interest and at varying angles of incidence. With optimal illumination wavelength and power, imaging depth in OCT is limited to about 2 to 3 mm in most nontransparent tissues, which is not as deep as ultrasound backscatter microscopy, micro-CT scanning, or MRI microscopy.<sup>3-7</sup> However, higher resolution optical imaging is performed at the expense of more limited imaging penetration.

Low-coherence light sources with operating wavelengths centered at 800 nm, such as the titanium:sapphire laser used in this study, can achieve broad spectral bandwidths and axial resolutions of less than 1  $\mu\text{m}$ .<sup>12</sup> These sources can achieve high imaging resolution; however, the 800-nm light is more scattered in biological tissue than 1300-nm light, a second commonly used wavelength in OCT.<sup>27</sup> Trade-offs exist between the use of 800- and 1300-nm light. Generally, the use of 800-nm light enables higher imaging resolution, but slightly less imaging penetration in highly scattering tissue, such as those tissues in this study. OCT imaging can be performed through small catheters, needles, and probes,<sup>28,29</sup> which could readily be used to assess the developing *in situ* murine embryo under even more physiological conditions.

OCT generates images based on amplitude variations in the detected signal, whereas Doppler OCT generates images based on frequency (phase) variations. Doppler OCT is analogous to Doppler ultrasound, but with much higher spatial and velocity resolution, and can determine real-time flow information within the developing cardiovascular system.<sup>30</sup> Doppler OCT measurements can determine velocity profiles at multiple depths and separate fluid-flow characteristics at different points. This technique has been used with SD-OCT to acquire real-time imaging of *in vivo* blood flow in the human retina,<sup>31</sup> along with many other dynamic applications. 3-D datasets have been acquired and processed to create volumetric reconstructions that avoid the visual overlap of fluid flows and apparent mixing in light-microscopy images of microfluidic devices.<sup>32</sup> The use of 3-D OCT and 3-D Doppler OCT can enable image reconstruction<sup>11,32</sup> of the tortuous and changing vascular network within the developing cardiovascular system, and may help identify dynamic function and flow defects in addition to the morphological defects found in CHDs.

In conclusion, high-resolution, real-time 3-D OCT imaging of the embryonic murine cardiovascular system can provide a unique and nondestructive means for investigating developing morphology and function. Further advances in the use of OCT will potentially enable assessment of functional cardiac parameters *in situ*. As our knowledgebase of functional genomics continues to grow, as does the reliance on the murine animal model to provide insight into human health and disease, investigative tools such as OCT are likely to play an important role in visualizing and quantifying the morphological and functional expression of the genome.

#### Acknowledgments

The authors thank Janet Sinn-Hanlon and Daniel Weber from the Beckman Institute for Advanced Science and Technology at the University of Illinois at Urbana-Champaign for providing help with the Analyze<sup>®</sup> software; and Jacquelyn Martin, Ian Atkinson, and Simon Schlachter for their research contributions to this study. This research was supported in part by the American Heart Association (0355396Z, S.A.B.) and the National Institutes of Health (NIBIB, 1 R01 EB00108-1, S.A.B.). Additional information can be found at <http://biophotonics.uiuc.edu>.

#### References

1. "Congenital heart defects in children fact sheet," American Heart Association, see <http://www.americanheart.org/children> (2004).
2. R. M. Brune, J. B. Bard, C. Dubreuil, E. Guest, W. Hill, M. Kaufman, M. Stark, D. Davidson, and R. A. Baldock, "A three-dimensional model of the mouse at embryonic day 9," *Dev. Biol.* **216**, 457–468 (1999).
3. T. M. Yelbuz, X. Zhang, M. A. Choma, H. A. Stadt, M. Zdanowicz, G. A. Johnson, and M. L. Kirby, "Images in cardiovascular medicine. Approaching cardiac development in three dimensions by magnetic resonance microscopy," *Circulation* **109**, 154–155 (2003).
4. J. E. Schneider, S. D. Bamforth, C. R. Farthing, K. Clarke, S. Neubauer, and S. Bhattacharya, "Rapid identification and 3D reconstruction of complex cardiac malformations in transgenic mouse embryos using fast gradient echo sequence magnetic resonance imaging," *J. Mol. Cell. Cardiol.* **35**, 217–222 (2003).
5. S. Brekke, E. Tegnander, H. G. Torp, and S. H. Eik-Nes, "Tissue Doppler gated (TDOG) dynamic three-dimensional ultrasound imaging of the fetal heart," *Ultrasound Obstet. Gynecol.* **24**, 192–198 (2004).
6. D. H. Turnbull, T. S. Bloomfield, H. S. Baldwin, F. S. Foster, and A. L. Joyner, "Ultrasound backscatter microscope analysis of early mouse embryonic brain development," *Proc. Natl. Acad. Sci. U.S.A.* **92**, 2239–2243 (1995).
7. A. J. Ewald, H. McBride, M. Reddington, S. E. Fraser, and R. Kerschmann, "Surface imaging microscopy, an automated method for visualizing whole embryo samples in three dimensions at high resolution," *Dev. Dyn.* **225**, 369–375 (2002).
8. J. Sharpe, U. Ahlgren, P. Perry, B. Hill, A. Ross, J. Hecksher-Sorensen, R. Baldock, and D. Davidson, "Optical projection tomography as a tool for 3D microscopy and gene expression studies," *Science* **296**, 541–545 (2002).
9. E. A. Jones, D. Crotty, P. M. Kulesa, C. W. Waters, M. H. Baron, S. E. Fraser, and M. E. Dickinson, "Dynamic *in vivo* imaging of postimplantation mammalian embryos using whole embryo culture," *Genesis* **28**, 228–235 (2002).
10. D. Huang, E. A. Swanson, C. P. Lin, J. S. Schuman, W. G. Stinson, W. Chang, M. R. Hee, T. Flotte, K. Gregory, C. A. Puliafito, and J. G. Fujimoto, "Optical coherence tomography," *Science* **254**, 1178–1181 (1991).
11. S. A. Boppart, B. E. Bouma, C. Pitris, G. J. Tearney, J. F. Southern, M. E. Brezinski, and J. G. Fujimoto, "Intraoperative assessment of microsurgery with three-dimensional optical coherence tomography," *Radiology* **208**, 81–86 (1998).
12. B. Povazay, K. Bizheva, A. Unterhuber, B. Hermann, H. Sallmann, A. F. Fercher, W. Drexler, A. Apolonski, W. J. Wadsworth, J. C. Knight, P. St. J. Russell, M. Vetterlein, and E. Scherzer, "Submicrometer axial resolution optical coherence tomography," *Opt. Lett.* **27**, 1800–1802 (2002).
13. S. A. Boppart, G. J. Tearney, B. E. Bouma, J. F. Southern, M. E. Brezinski, and J. G. Fujimoto, "Noninvasive assessment of the developing *Xenopus* cardiovascular system using optical coherence tomography," *Proc. Natl. Acad. Sci. U.S.A.* **94**, 4256–4261 (1997).
14. T. M. Yelbuz, M. A. Choma, L. Thrane, M. L. Kirby, and J. A. Izatt, "Optical coherence tomography: a new high-resolution imaging technology to study cardiac development in chick embryos," *Circulation* **106**, 2771–2774 (2002).
15. *Cardiovascular Physiology in the Genetically Engineered Mouse (Developments in Cardiovascular Medicine)*, B. D. Hoit and R. A. Walsh, Eds., Springer, Berlin (1998).
16. *Mouse Models of Human Cancer*, E. C. Holland, Ed., Wiley-Liss, New York (2004).
17. M. A. Suckow, P. Danneman, and C. Brayton, *The Laboratory Mouse*, CRC Press, Boca Raton, FL (2000).
18. A. L. Oldenburg, D. L. Marks, and S. A. Boppart, "Fast-Fourier-domain delay line for *in vivo* optical coherence tomography with a polygonal scanner," *Appl. Opt.* **42**, 4606–4611 (2003).
19. M. A. Choma, M. V. Sarunic, C. Yang, and J. A. Izatt, "Sensitivity advantage of swept source and Fourier domain optical coherence tomography," *Opt. Express* **11**, 2183–2189 (2003).
20. D. L. Marks, J. J. Reynolds, and S. A. Boppart, "Autofocus algorithm for dispersion correction in optical coherence tomography," *Appl. Opt.* **42**, 3038–3046 (2003).
21. J. F. de Boer, B. H. Park, M. C. Pierce, G. J. Tearney, and B. E. Bouma, "Improved signal-to-noise ratio in spectral-domain compared with time-domain optical coherence tomography," *Opt. Lett.* **28**, 2067–2069 (2003).
22. R. A. Leitgeb, C. K. Hitzenberger, and A. F. Fercher, "Performance of Fourier domain vs. time domain optical coherence tomography," *Opt. Express* **11**, 889–894 (2003).
23. M. J. MacLennan and B. B. Keller, "Umbilical arterial blood flow in the mouse embryo during development and following acutely increased heart rate," *Ultrasound Med. Biol.* **25**, 361–370 (1999).
24. C. K. Phoon, O. Aristizabal, and D. H. Turnbull, "40 MHz Doppler characterization of umbilical and dorsal aortic blood flow in the early mouse embryo," *Ultrasound Med. Biol.* **26**, 1275–1283 (2000).
25. C. Yang, "Molecular contrast optical coherence tomography: a review," *Photochem. Photobiol.* **81**, 215–237 (2005).
26. S. A. Boppart, A. L. Oldenburg, C. Xu, and D. L. Marks, "Optical probes and techniques for molecular contrast enhancement in coherence imaging," *J. Biomed. Opt.* **10**, 041208 (2005).
27. B. E. Bouma, G. J. Tearney, I. P. Bilinsky, B. Golubovic, and J. G. Fujimoto, "Self-phase-modulated Kerr-lens mode-locked Cr:forsterite laser source for optical coherence tomography," *Opt. Lett.* **21**, 1839–1841 (1996).
28. S. A. Boppart, C. Pitris, G. J. Tearney, and J. G. Fujimoto, "Forward-imaging instruments for optical coherence tomography," *Opt. Lett.* **22**, 1618–1620 (1997).
29. X. Li, T. Ko, C. Pitris, and J. G. Fujimoto, "Imaging needle for optical coherence tomography," *Opt. Lett.* **25**, 1520–1522 (2000).
30. A. M. Rollins, S. Yazdanfar, J. K. Barton, and J. A. Izatt, "Real-time *in vivo* color Doppler optical coherence tomography," *J. Biomed. Opt.* **7**(1), 123–129 (2002).
31. B. R. White, M. C. Pierce, N. Nassif, B. Cense, B. H. Park, G. J. Tearney, B. E. Bouma, T. C. Chen, and J. F. de Boer, "In vivo dynamic human retinal blood flow imaging using ultra-high-speed spectral domain optical Doppler tomography," *Opt. Express* **11**, 3490–3497 (2003).
32. C. Xi, D. L. Marks, D. S. Parikh, L. Raskin, and S. A. Boppart, "Structural and functional imaging of 3D microfluidic mixers using optical coherence tomography," *Proc. Natl. Acad. Sci. U.S.A.* **101**, 7516–7521 (2004).